ACS Energy LETTERS

http://pubs.acs.org/journal/aelccp

Letter

Simply Fabricatable Reference Electrode for Studying Li Metal Interfaces *Operando*

Jacob Florian, Hao Lyu, Luca Mondonico, Yepin Zhao, Jane K.J. Lee, Amanda L. Musgrove, Yi Cui, Robert L. Sacci, and Zhenan Bao*

Cite This: *ACS Energy Lett.* 2026, 11, 1835−1840

Read Online

ACCESS | Metrics & More | Article Recommendations | Supporting Information

ABSTRACT: Reference electrodes are essential for studying Li metal interfaces, yet their integration into coin cells remains challenging due to geometric constraints and assembly complexity. Here, we present a simple three-electrode coin cell design in which a thin Cu film is evaporated directly onto a trilayer PP/PE/PP separator, forming a conductive and flexible *in situ* current collector. The microporous Cu preserves separator porosity and pressure uniformity, avoiding artifacts introduced by wire- or mesh-type references. It is easily activated by Li plating and provides stable potentials for over 10 days in ether-based electrolytes without affecting Coulombic efficiency (>99%) or Li deposition morphology. *Operando* measurements using this design reveal electrode-specific impedance evolution and voltage responses otherwise obscured in two-electrode setups, uncovering a correlation between the SEI resistance and electrolyte ionic conductivity. This microporous Cu reference electrode offers a robust and accessible platform for characterizing reactive interfaces under realistic cycling conditions.

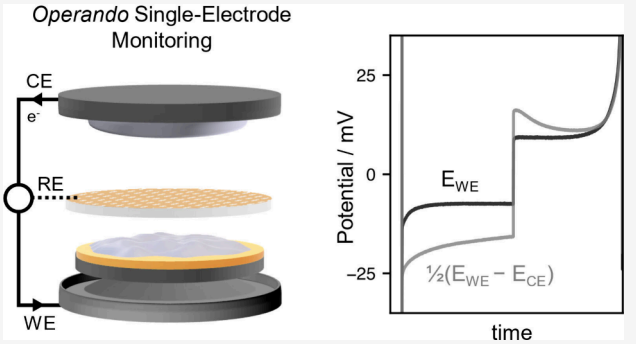

Reference electrodes enable single-electrode potential control which is essential for disentangling the complex phenomena that unfold at reactive electrodes.[1−3] This is particularly true for lithium metal, where high chemical reactivity, solid electrolyte interphase (SEI) formation and rupture, roughening, and void growth during stripping can all occur concurrently and feedback on one another.[4−7] Despite the apparent advantages of single-electrode monitoring, most experimental studies of Li metal anodes still rely on two-electrode coin cells. Coin cells are easy to assemble reproducibly, require minimal hardware, and are ideal for screening the electrochemical performance of novel electrodes and electrolyte chemistries. Yet, this format prevents direct attribution of features in voltage or impedance to a specific interface, limiting their diagnostic and mechanistic utility. Even in symmetric cells, the counter electrode can dominate and convolute the electrochemical response, masking the true behavior at the interface of interest.

Three-electrode configurations overcome this limitation in principle, but their practical implementation in coin cells remains rare. Most existing approaches thread a Li wire or mesh into the coin cell stack or bring in an external lead that disturbs the internal geometry. These interventions create local variations in stack pressure and ionic transport pathways, which lead to geometric asymmetries that are known to influence overpotentials and deposition morphology.[8] As a result, artifacts from the reference itself can contaminate voltage and impedance readouts, compromising the very measurements the reference is intended to enable.[9−12] The fabrication burdens can also be high. Many designs require multistep coating of active reference materials, laser-cut parts, custom gaskets, or expensive materials, all of which erode the reproducibility and speed advantages of coin cells.[12]

A concise comparison of reference electrode designs is provided in Table 1. Li metal wires are attractive because Li/Li^+ defines a simple and widely understood potential and the assembly is trivial (i.e., pressing Li foil onto a conductor). However, in liquid electrolytes the Li reference continuously reacts, leading to potential drift, while the wire geometry concentrates pressure and distorts electric fields in the stack.[1,12] Alloy and insertion references (e.g., lithium titanate and lithium iron phosphate) offer superior potential stability over days to weeks, but the typical fabrication—slurry coating on a mesh or foil, drying, and integration—adds complexity and thickness that can disrupt the stack. Microelectrodes and meshes mitigate some asymmetry, yet their thickness relative to the separator can still introduce pressure gradients and selectively block ion transport.[12] The potential stability,

Received: October 23, 2025
Revised: December 7, 2025
Accepted: December 31, 2025
Published: January 10, 2026

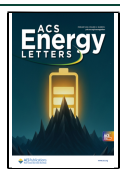

https://doi.org/10.1021/acsenergylett.5c03496
ACS Energy Lett. 2026, 11, 1835−1840

Table 1. Comparison of Existing Reference Electrode Designs for Li Coin Cells

	Fabrication	Stability	Geometric Impact	Examples
Li metal wire	simple assembly	long-term potential drift	localized pressure geometric asymmetry	13−17
Li alloy/insertion wires	requires alloy formation or coatings	stable potential	localized pressure geometric asymmetry	18−21
Coated mesh	requires surface treatment	stable potential	localized pressure increased internal resistance	22−24
Separator-mounted film	complex fabrication	stable potential	minimal impact	25
Microelectrodes	fragile handling	long-term potential drift	some localized pressure	26, 27

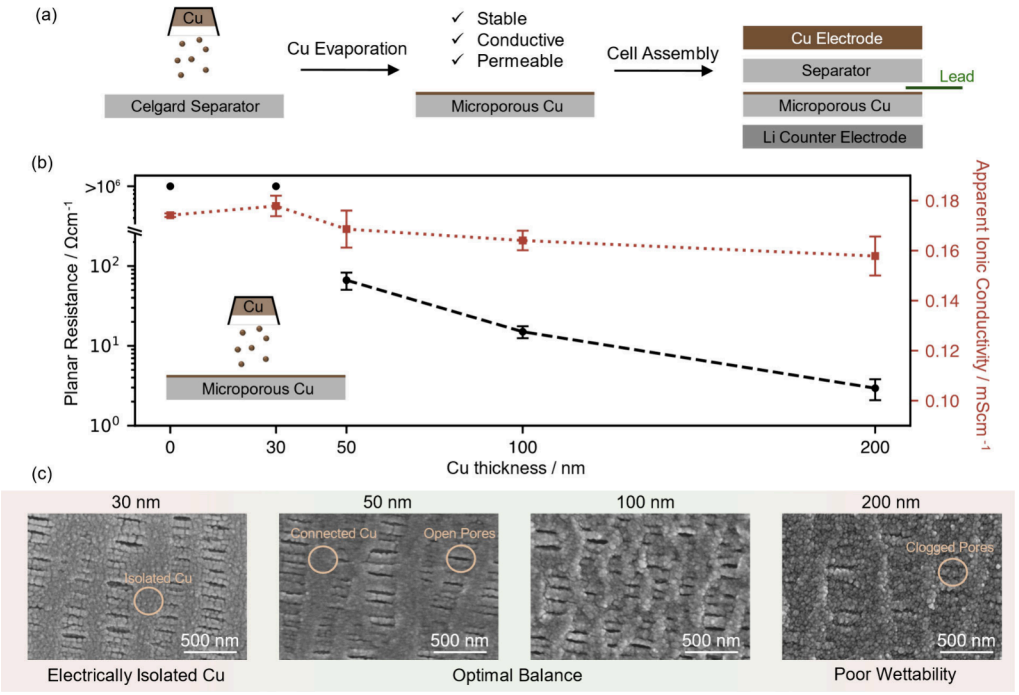

Figure 1. Fabrication and characterization of the microporous Cu reference electrode. (a) Thermal evaporation of Cu onto a Celgard H1409 substrate creates a conductive and permeable surface layer. It can be integrated as a stand-alone current collector in the coin cell stack. (b) Effect of Cu thickness on in-plane resistance (black) and apparent ionic conductivity of the cell stack in 1 M LiFSI F5DEE (red). The apparent ionic conductivity was calculated from the bulk resistance measured in a coin cell containing two microporous Cu separators placed between stainless-steel blocking electrodes. (c) SEM images showing the surface morphology of the electrode at different Cu thickness.

geometry, and fabrication burden must be considered when choosing reference electrodes. Currently, no easily fabricatable and geometrically neutral reference electrode exists for monitoring the Li metal interfaces.

To resolve these challenges, we designed a reference that is *geometrically invisible* to the coin-cell stack yet capable of artifact-free single-electrode monitoring. The concept is simple: evaporate a thin film of copper directly onto a commercial PP/PE/PP separator and use this metalized separator as the reference electrode (Figure S1). Because the copper resides on the separator surface, the film conforms to its native porosity and thickness, preserving the planar pressure distribution and ion-transport pathways present in conventional coin cells.[25,28] Because the reference is integrated into the separator, no bulky lead or wire intrudes into the active electrode area. Instead, a fine external lead is attached so that it exits the coin-cell without crossing the electrode footprint (Figure S2). And because the copper can be lithium-plated *in situ* using a brief, low-capacity step, the reference potential can be set to Li/Li^+ without introducing a separate Li object into the stack. In short, this microporous Cu reference electrode acts as both an ionic conduit and reference substrate, seamlessly integrating into the coin-cell form factor.

We optimized the evaporated copper thickness to balance the in-plane conductivity with preserved porosity (Figure 1). A 30 nm Cu coating appeared visually continuous but was electrically discontinuous: SEM revealed disconnected nanoislands (Figure 1c), and its lateral conductance was unmeasurable (Figure 1b). At 50 nm, the film provided an in-plane resistance of ∼66 Ω cm^{-1}, while SEM confirmed that the pores remained open mimicking the pristine separator (Figure S3). Increasing the Cu thickness to 100 nm reduced the resistance further to ∼15 Ω cm^{-1} and continued to preserve the pore architecture (Figure 1c). Increasing to 200 nm continued to lower the in-plane resistance (∼2.8 Ω cm^{-1}) but began to occlude pores. Notably, at 200 nm the electrolyte failed to wet the separator immediately, signaling that ion transport was compromised. The through-plane ionic resistance measurements across separators with different Cu thicknesses were indistinguishable within experimental error from those of the pristine Celgard H1409 separator (Figure 1b, Figure S4), indicating that the Cu does not measurably impede

https://doi.org/10.1021/acsenergylett.5c03496
ACS Energy Lett. 2026, 11, 1835−1840

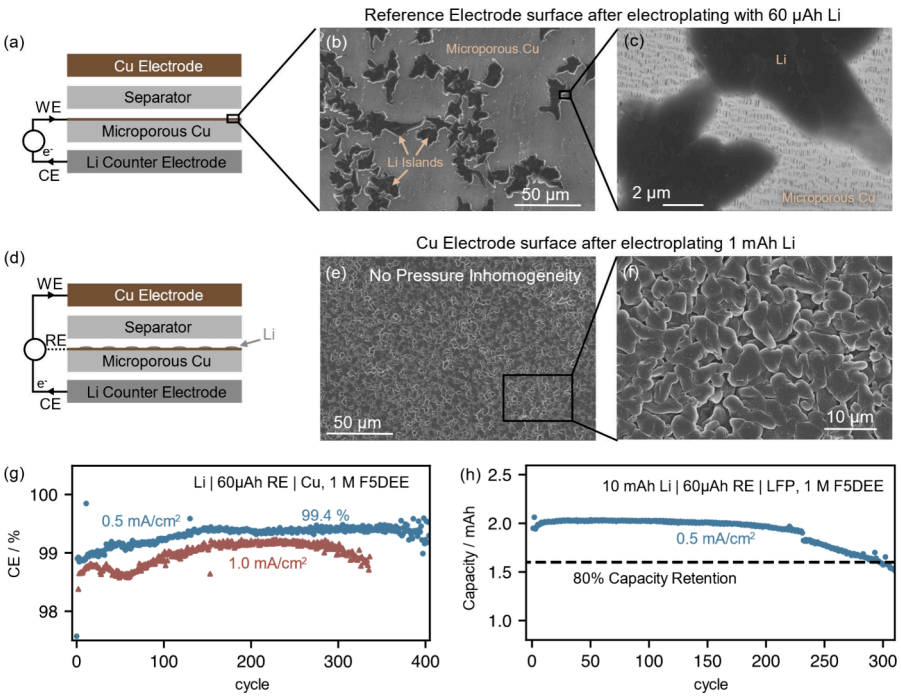

Figure 2. Morphology and performance of three-electrode cells using the microporous Cu reference electrode in a 1 M LiFSI F5DEE electrolyte. (a) Cell stack for Li plating on the microporous reference electrode from the bulk Li counter electrode. (b, c) Microporous Cu surface after electroplating 60 μAh of Li at 100 μAcm^{-2} from the Li counter electrode. Backscatter SEM in (c) reveals the dark Li islands atop the light microporous Cu surface. (d) Cell stack for three electrode LiCu cell operation. (e, f) SEM images of the Cu working electrode after plating 1 mAh of Li in the three-electrode cell. (g) Long cycling Coulombic efficiency during cycling at 1 mAh capacity in the three-electrode half cells at 0.5 mAcm^{-2} (blue) and 1.0 mAcm^{-2} (red). (h) Capacity curve during cycling in a three electrode 10 mAh Li|LFP full cell. The stepwise drop at cycle 230 was caused by a prolonged resting period following a power outage.

bulk ion transport. From these results we selected 50 nm as a conservative standard because it is conductive for potential readout yet thin enough to preserve wetting and ionic conduction.

The coin-cell assembly is identical to the standard practice except for adding the microporous Cu reference electrode beneath a slightly oversized pristine separator (Figure 2a). A 25 μm wire lead is attached to the Cu film at the separator rim such that it contacts the conductive substrate without extending into the active electrode area (Figure S2). This preserves a planar, homogeneous stack and avoids a local pressure concentration. After assembly and wetting, the microporous Cu reference is activated by plating 60 μAh cm^{-2} of Li onto the Cu film *in situ* (Figure S5). SEM images of the plated microporous Cu electrode show evenly distributed Li islands across the separator surface (Figure 2b), while backscatter imaging reveals large dark Li features on the lighter microporous Cu-coated scaffold (Figure 2c), confirming that Li nucleates on the copper without disrupting the separator microstructure. Critically, the impedance measured before and after this activation step shows no change in bulk conductivity (Figures S6 and S7), indicating that the Li islands do not meaningfully block ion transport. A complete description and video of the fabrication and assembly are given in Movie S1.

To quantify the performance of three-electrode coin cells using the microporous Cu reference electrode, we used 1 M LiFSI in 2-(2-(2,2-difluoroethoxy)ethoxy)-1,1,1-trifluoroethane (F5DEE) as the electrolyte. This electrolyte was chosen for two reasons that pull it in opposite experimental directions. First, it exhibits high Coulombic efficiency (~99.5%),[29] which makes any performance degradation caused by the reference electrode immediately apparent. Second, it has low ionic conductivity compared to common ethers (0.11 mS/cm within the separator),[29] which makes performance more sensitive to separator spacing and wetting. In such an electrolyte, intrusive reference electrode designs significantly degrade performance. After plating 60 μAh of Li in F5DEE, the microporous Cu potential remains stable for >50 days (Figure S8). For benchmarking breadth, we also examined 1 M LiFSI in 1,2-dimethoxyethane (DME) and carbonate-based LP40, in which the microporous Cu potential remained stable for 10 days, reflecting the expected solvent-dependent corrosion of small Li features on copper (Figures S9–S11).

A central question is whether the microporous Cu reference perturbs the Li deposition on the working electrode. Conventional wire and mesh references can locally distort the ion flux or pressure distribution, leading to nonuniform Li plating. In contrast, Li deposition on Cu in three-electrode coin cells with the microporous Cu reference remained spatially homogeneous (Figure 2d–f) and was indistinguishable from the morphology observed in pristine two-electrode controls (Figure S12). Moreover, interfacial impedance measurements were not distorted by slight reference electrode misalignment (Figure S13) or small differences in stack height (Figure S14), demonstrating a tolerance to mechanical disturbances.

Beyond morphology, long-term cycling provides a stringent performance metric. Three-electrode Li|Cu cells, cycled to 1 mAh at 0.5 and 1 mA cm^{-2}, delivered Coulombic efficiencies of 99.4% and 99.1%, respectively, with continuous operation sustained for as many as 400 cycles (Figure 2g). This matches

https://doi.org/10.1021/acsenergylett.5c03496
ACS Energy Lett. 2026, 11, 1835−1840

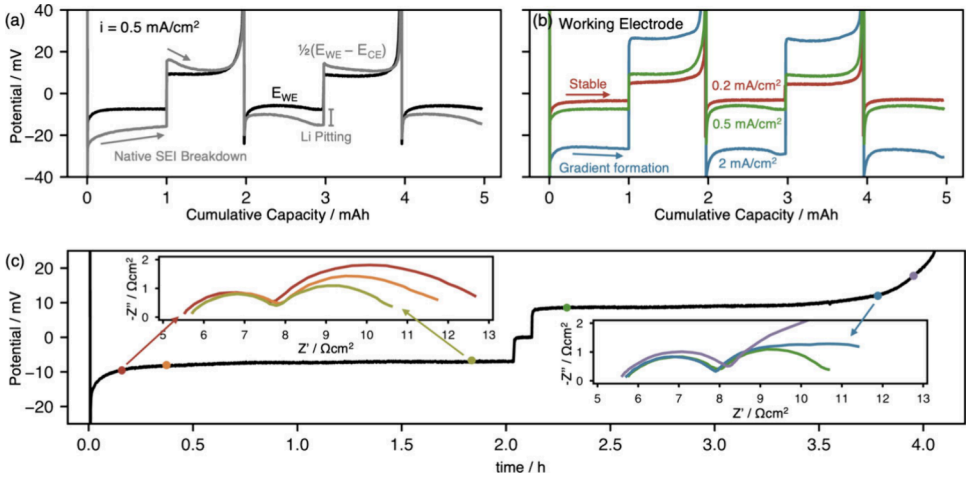

Figure 3. Electrochemical performance of three-electrode coin cells using the microporous Cu reference electrode. (a) Voltage trace for the first three cycles of Li plating in three-electrode LiCu cells (black) compared to two-electrode cells (gray) at 0.5 $mAcm^{-2}$ for 1 mAh. (b) Voltage trace of the Cu working electrode in three-electrode cells at 0.2, 0.5, and 2.0 $mAcm^{-2}$. (c) EIS snapshots during the first cycle of Li metal plating and stripping from Cu at 0.5 $mAcm^{-2}$.

the level of performance observed in two-electrode cells,[29] demonstrating that the inclusion of a microporous Cu reference does not affect electrochemical performance. Extending to full cells, Cu||LFP anode-free three-electrode coin cells cycled at 0.5 mA/cm^2 delivered an average CE of ~99.3% (Figure S15). The three-electrode LFP coin cell paired with a 10 mAh electroplated Li metal anode retained 80% of its initial capacity after 300 cycles (Figure 2h), and its voltage trace is shown in Figure S16. When this cell was disassembled after shorting at >300 cycles, the microporous Cu reference electrode did not show any signs of damage or degradation beyond Li corrosion (Figure S17). While maximizing the cycle life is not the purpose of the reference electrode, the ability to achieve robust cycling in a three-electrode coin cell confirms that the microporous Cu does not compromise stack mechanics or transport.

With nonintrusivity established, the diagnostic benefits of electrode-resolved measurements become clear. Side-by-side voltage traces from a conventional Li||Cu two-electrode cell and a three-electrode cell with a microporous Cu reference electrode reveal the importance of direct single-electrode monitoring (Figure 3a). In the two-electrode voltage trace, the apparent half-cell potential ($\frac{E_{WE} - E_{CE}}{2}$) starts near ~20 mV and decays toward ~15 mV during the first half-cycle, reflecting the large contributions from native SEI breakdown at the Li counter electrode. The overpotential increases toward the end of plating and then decreases during stripping, reflecting pit formation and dendrite growth on the Li counter electrode.[13,30,31] In the three-electrode configuration, the working-electrode potential is isolated: during the first plating step, it rapidly reaches a stable potential of ~7 mV and appears symmetric between plating and stripping. The true overpotential at the working electrode is overestimated in two electrode cells, demonstrating the advantage of single-electrode monitoring.

The microporous Cu reference electrode enables *operando* characterization of Li interfaces across a wide range of current densities. Figure 3b shows voltage traces of Li plating and stripping from the Cu working electrode at progressively increasing currents. At 0.2−0.5 mA/cm^2, the working electrode response is stable and nearly symmetric between plating and stripping. At higher current density (2 mA/cm^2), the voltage displays a progressive rise in overpotential with plating time and cycle number, consistent with the buildup of concentration gradients in both the bulk electrolyte and the electrode interface. In a two-electrode cell, such effects are easily obscured by the response of the Li counter electrode. The microporous Cu reference electrode also ensures single-electrode accuracy during voltammetry, where IR drop and counterelectrode overpotentials become significant at fast scan rates (Figure S18).

Electrode-resolved impedance is crucial for capturing the interfacial phenomena (Figure 3c). Snapshots during Li plating show a decrease in interfacial impedance as Li deposits. Upon reversal to stripping, the low-frequency semicircle grows as Li near the current collector is depleted. Because the counter electrode is excluded from the measurement, these spectra reflect the intrinsic evolution of the plated-Li interface—information otherwise obscured in two-electrode cells.

We also compared the interfacial resistance of electroplated Li using two- and three-electrode measurements (Figure 4). Twelve electrolytes, ranging from conventional carbonates to fluorinated ethers, were tested by electroplating 1 mAh of Li onto a Cu working electrode in a Li||Cu coin cell (Figure S19). Li was deposited from a bulk counter electrode at a low current density (0.2 mA cm^{-2}) to minimize concentration gradients, and impedance spectra were collected immediately after plating in both cell configurations (Figure S20−S23, Tables S1 and S2).

The contrast between two- and three-electrode measurements underscores the importance of *operando* single-electrode resolution. In the two-electrode mode, the impedance spectrum is dominated by contributions from the native SEI on the bulk Li source, obscuring any electrolyte-dependent trends (Figure 4a). In the three-electrode configuration, the isolated response of the electroplated Li reveals a clear negative correlation between the electrolyte ionic conductivity (Table S1) and SEI resistance (Figure 4b, Table S2). This observation supports the role of solvent-assisted ion transport within the SEI, as suggested in our prior work,[32] and demonstrates the utility of the microporous Cu reference electrode for practical, *operando* characterization of Li metal interfaces.

https://doi.org/10.1021/acsenergylett.5c03496
ACS Energy Lett. 2026, 11, 1835−1840

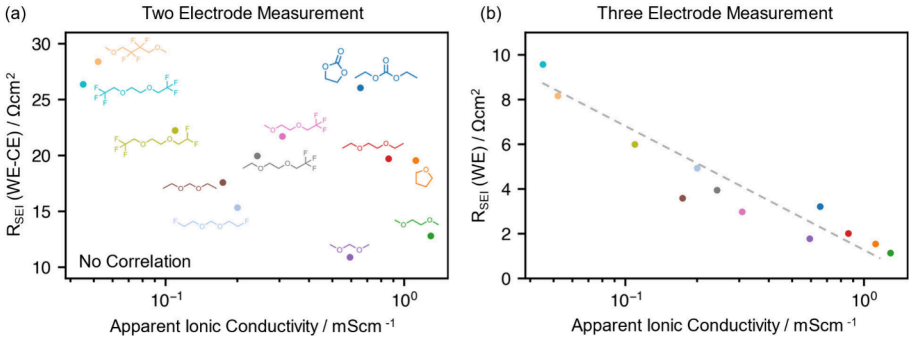

Figure 4. SEI resistance (R_{SEI}) as a function of electrolyte conductivity after plating 1 mAh/cm^2 Li in a LiCu three electrode cell with various solvents, each containing 1 M LiFSI. (a) In a two-electrode EIS measurement, there is no correlation between R_{SEI} and the electrolyte's ionic conductivity. (b) In a three-electrode EIS measurement, the impedance of the electroplated Li on Cu is isolated from the bulk Li source, revealing a correlation between R_{SEI} and the electrolyte's ionic conductivity. The apparent ionic conductivity of each electrolyte is measured in a Celgard H1409 separator.

The principal limitation of this design is the finite lifetime of a Li-plated reference. Small Li islands on copper slowly corrode in most liquid electrolytes.[33] Over weeks to months, the open-circuit potential can drift as the metallic Li inventory diminishes (Figure S7). This limitation is inherent to Li-metal references, and it can be mitigated by periodic replating of a small amount of Li or by replacing the plated-Li reference with a thin insertion reference (e.g., LFP or LTO) deposited onto the separator. The latter would extend the stable potential window at the cost of additional processing steps that the current design intentionally avoids. In our view, the simplicity and fidelity of the microporous Cu reference electrode make it ideally suited to short- and medium-duration *operando* diagnostics, which is precisely where two-electrode convolution has muddied interpretation.

In summary, the microporous Cu separator-integrated reference electrode brings three-electrode capability to coin cells without sacrificing the virtues that have made coin cells so widely adopted. A single thin-film metallization step produces a conductive, porous separator that, once lightly lithiated, functions as a stable Li/Li$^+$ reference. The design preserves homogeneous pressure and ion-transport pathways, does not degrade Coulombic efficiency or cycling stability, and yields electrode-resolved voltage and impedance signatures that illuminate interfacial processes otherwise obscured in two-electrode measurements. By lowering the barrier to artifact-free three-electrode experiments, this platform expands the toolbox for the mechanistic studies of reactive interfaces under realistic cycling conditions.

■ ASSOCIATED CONTENT

Supporting Information

The Supporting Information is available free of charge at https://pubs.acs.org/doi/10.1021/acsenergylett.5c03496.

Experimental methods, details of microporous Cu fabrication, details of three-electrode cell preparation, impedance measurements before and after Li plating on microporous Cu, reference electrode potential drift measurements, Li morphology comparison to two-electrode coin cells, effects of mechanical disturbances, voltage trace for three-electrode full cells, pictures of microporous Cu reference electrode after cycling, three-electrode cyclic voltammetry, voltage trace and impedance measurements for select electrolytes, fitting parameters for Nyquist plots, and apparent ionic conductivity calculation (PDF)

Supporting video (MP4)

■ AUTHOR INFORMATION

Corresponding Author

Zhenan Bao − *Department of Chemical Engineering, Stanford University, Stanford, California 94305, United States;* orcid.org/0000-0002-0972-1715; Email: zbao@stanford.edu

Authors

Jacob Florian − *Department of Chemical Engineering, Stanford University, Stanford, California 94305, United States;* orcid.org/0000-0003-1895-8463

Hao Lyu − *Department of Chemical Engineering, Stanford University, Stanford, California 94305, United States;* orcid.org/0000-0001-7393-2456

Luca Mondonico − *Department of Materials Science and Engineering, Stanford University, Stanford, California 94305, United States*

Yepin Zhao − *Department of Chemical Engineering, Stanford University, Stanford, California 94305, United States;* orcid.org/0000-0001-9988-0949

Jane K.J. Lee − *Department of Structural Biology, Stanford University, Stanford, California 94305, United States*

Amanda L. Musgrove − *Chemical Sciences Division, Oak Ridge National Laboratory, Oak Ridge, Tennessee 37830, United States;* orcid.org/0009-0002-2091-0389

Yi Cui − *Department of Materials Science and Engineering, Stanford University, Stanford, California 94305, United States;* orcid.org/0000-0002-6103-6352

Robert L. Sacci − *Chemical Sciences Division, Oak Ridge National Laboratory, Oak Ridge, Tennessee 37830, United States;* orcid.org/0000-0002-0073-5221

Complete contact information is available at: https://pubs.acs.org/10.1021/acsenergylett.5c03496

Notes

The authors declare no competing financial interest.

■ ACKNOWLEDGMENTS

This work is supported by the US Department of Energy, under the Assistant Secretary for Energy Efficiency and

https://doi.org/10.1021/acsenergylett.5c03496
ACS Energy Lett. 2026, 11, 1835−1840

Renewable Energy, Vehicle Technologies Office, the Battery Materials Research Program and Battery500 Consortium. SEM imaging was performed at the Stanford Nano Shared Facilities (SNSF), supported by the National Science Foundation under award ECCS-2026822. J.F. acknowledges support from the NSF Graduate Research Fellowship for graduate studies at Stanford.

REFERENCES

(1) Zhang, Z.; Li, Y.; Min, X.; Ren, D.; Song, Y.; Wang, L.; Zhao, H.; He, X. Enhancing Precision and Durability of Built-In Cu-Li Reference Electrodes in Lithium-Ion Batteries: A Critical Review. *ACS Energy Lett.* **2024**, *9* (11), 5647−5669.

(2) Cengiz, E. C.; Rizell, J.; Sadd, M.; Matic, A.; Mozhzhukhina, N. Review—Reference Electrodes in Li-Ion and Next Generation Batteries: Correct Potential Assessment, Applications and Practices. *J. Electrochem. Soc.* **2021**, *168* (12), 120539.

(3) Rangarajan, S. P.; Sarkar, S.; Barsukov, Y.; Mukherjee, P. P. 3ε-A Versatile Operando Analytics Toolbox in Energy Storage. *ACS Omega* **2021**, *6* (49), 33284−33292.

(4) Lin, D.; Liu, Y.; Cui, Y. Reviving the Lithium Metal Anode for High-Energy Batteries. *Nat. Nanotechnol.* **2017**, *12* (3), 194−206.

(5) Liu, H.; Cheng, X.-B.; Xu, R.; Zhang, X.-Q.; Yan, C.; Huang, J.-Q.; Zhang, Q. Plating/Stripping Behavior of Actual Lithium Metal Anode. *Adv. Energy Mater.* **2019**, *9* (44), 1902254.

(6) Kasemchainan, J.; Zekoll, S.; Spencer Jolly, D.; Ning, Z.; Hartley, G. O.; Marrow, J.; Bruce, P. G. Critical Stripping Current Leads to Dendrite Formation on Plating in Lithium Anode Solid Electrolyte Cells. *Nat. Mater.* **2019**, *18* (10), 1105−1111.

(7) Sanchez, A. J.; Dasgupta, N. P. Lithium Metal Anodes: Advancing Our Mechanistic Understanding of Cycling Phenomena in Liquid and Solid Electrolytes. *J. Am. Chem. Soc.* **2024**, *146* (7), 4282−4300.

(8) Pande, V.; Abbasalinejad, A.; Hammond, J.; Christensen, J.; Kim, S. U. Impact of Size and Position of Lithium Metal Reference Electrodes on the Measurement of Lithium-Plating Overpotential. *J. Electrochem. Soc.* **2021**, *168* (9), 090534.

(9) Li, Y.; Han, X.; Feng, X.; Chu, Z.; Gao, X.; Li, R.; Du, J.; Lu, L.; Ouyang, M. Errors in the Reference Electrode Measurements in Real Lithium-Ion Batteries. *J. Power Sources* **2021**, *481*, 228933.

(10) Ender, M.; Weber, A.; Ellen, I.-T. Analysis of Three-Electrode Setups for AC-Impedance Measurements on Lithium-Ion Cells by FEM Simulations. *J. Electrochem. Soc.* **2011**, *159* (2), A128−A136.

(11) Ender, M.; Illig, J.; Ivers-Tiffée, E. Three-Electrode Setups for Lithium-Ion Batteries: I. Fem-Simulation of Different Reference Electrode Designs and Their Implications for Half-Cell Impedance Spectra. *J. Electrochem. Soc.* **2017**, *164* (2), A71−A79.

(12) Raccichini, R.; Amores, M.; Hinds, G. Critical Review of the Use of Reference Electrodes in Li-Ion Batteries: A Diagnostic Perspective. *Batteries* **2019**, *5* (1), 12.

(13) Wood, K. N.; Kazyak, E.; Chadwick, A. F.; Chen, K.-H.; Zhang, J.-G.; Thornton, K.; Dasgupta, N. P. Dendrites and Pits: Untangling the Complex Behavior of Lithium Metal Anodes through Operando Video Microscopy. *ACS Cent. Sci.* **2016**, *2* (11), 790−801.

(14) Dutta, A.; Kubo, Y.; Nagataki, A.; Matsushita, K. Deciphering the Dynamic Processes at the Electrode-Electrolyte Interface for Stable Deposition of Lithium. *ACS Appl. Mater. Interfaces* **2023**, *15* (12), 15467−15477.

(15) Seok, J.; Gannett, C. N.; Yu, S.-H.; Abruña, H. D. Understanding the Impacts of Li Stripping Overpotentials at the Counter Electrode by Three-Electrode Coin Cell Measurements. *Anal. Chem.* **2021**, *93* (46), 15459−15467.

(16) Rangarajan, S. P.; Barsukov, Y.; Mukherjee, P. P. In Operando Signature and Quantification of Lithium Plating. *J. Mater. Chem. A* **2019**, *7* (36), 20683−20695.

(17) Minter, R. D.; Juarez-Robles, D.; Fear, C.; Barsukov, Y.; Mukherjee, P. P. Three-Electrode Coin Cell Preparation and Electrodeposition Analytics for Lithium-Ion Batteries. *J. Vis. Exp. JoVE* **2018**, No. 135, No. e57735.

(18) Kalaga, K.; Rodrigues, M.-T. F.; Abraham, D. P. In Situ Lithiated Reference Electrode: Four Electrode Design for In-Operando Impedance Spectroscopy. *J. Vis. Exp. JoVE* **2018**, No. 139, No. e57375.

(19) Chien, Y.-C.; Brandell, D.; Lacey, M. J. Towards Reliable Three-Electrode Cells for Lithium-Sulfur Batteries. *Chem. Commun.* **2022**, *58* (5), 705−708.

(20) Yi, S.; Wang, B.; Chen, Z.; Wang, R.; Wang, D. A Study on LiFePO4/Graphite Cells with Built-in Li4Ti5O12 Reference Electrodes. *RSC Adv.* **2018**, *8* (33), 18597−18603.

(21) Juarez-Robles, D.; Chen, C.-F.; Barsukov, Y.; Mukherjee, P. P. Impedance Evolution Characteristics in Lithium-Ion Batteries. *J. Electrochem. Soc.* **2017**, *164* (4), A837.

(22) Epding, B.; Broda, A.; Rumberg, B.; Jahnke, H.; Kwade, A. Development of Durable 3-Electrode Lithium-Ion Pouch Cells with LTO Reference Mesh: Aging and Performance Studies. *J. Electrochem. Soc.* **2019**, *166* (8), A1550.

(23) Costard, J.; Ender, M.; Weiss, M.; Ivers-Tiffée, E. Three-Electrode Setups for Lithium-Ion Batteries. *J. Electrochem. Soc.* **2017**, *164* (2), A80.

(24) Rutz, D.; Bauer, I.; Brauchle, F.; Jacob, T. Designing a Reference Electrode - An Approach to Fabricate Laser Perforated Reference Electrodes for Lithium-Ion Batteries. *Electrochim. Acta* **2023**, *441*, 141768.

(25) Koch, B. J.; Gao, J.; Zhang, A.; Taha, R.; Garrick, T. R. A Versatile Reference Electrode for Lithium Ion Battery Use. *J. Electrochem. Soc.* **2025**, *172* (1), 013507.

(26) Solchenbach, S.; Pritzl, D.; Kong, E. J. Y.; Landesfeind, J.; Gasteiger, H. A. A Gold Micro-Reference Electrode for Impedance and Potential Measurements in Lithium Ion Batteries. *J. Electrochem. Soc.* **2016**, *163* (10), A2265.

(27) Zhou, J.; Notten, P. H. L. Development of Reliable Lithium Microreference Electrodes for Long-Term In Situ Studies of Lithium-Based Battery Systems. *J. Electrochem. Soc.* **2004**, *151* (12), A2173.

(28) Wu, H.; Zhuo, D.; Kong, D.; Cui, Y. Improving Battery Safety by Early Detection of Internal Shorting with a Bifunctional Separator. *Nat. Commun.* **2014**, *5* (1), 5193.

(29) Yu, Z.; Rudnicki, P. E.; Zhang, Z.; Huang, Z.; Celik, H.; Oyakhire, S. T.; Chen, Y.; Kong, X.; Kim, S. C.; Xiao, X.; Wang, H.; Zheng, Y.; Kamat, G. A.; Kim, M. S.; Bent, S. F.; Qin, J.; Cui, Y.; Bao, Z. Rational Solvent Molecule Tuning for High-Performance Lithium Metal Battery Electrolytes. *Nat. Energy* **2022**, *7* (1), 94−106.

(30) DrvaričTalian, S.; Kapun, G.; Moškon, J.; Dominko, R.; Gaberšček, M. Operando Impedance Spectroscopy with Combined Dynamic Measurements and Overvoltage Analysis in Lithium Metal Batteries. *Nat. Commun.* **2025**, *16* (1), 2030.

(31) Shi, F.; Pei, A.; Boyle, D. T.; Xie, J.; Yu, X.; Zhang, X.; Cui, Y. Lithium Metal Stripping beneath the Solid Electrolyte Interphase. *Proc. Natl. Acad. Sci. U. S. A.* **2018**, *115* (34), 8529−8534.

(32) Florian, J.; Lyu, H.; Choi, I. R.; Mondonico, L.; Lam, S.; Zhao, Y.; Kim, M.-J.; Westover, A.; Cui, Y.; Sacci, R. L.; Bao, Z. Revealing Solvent-Assisted Li+ Transport in the Solid Electrolyte Interphase Operando. *J. Am. Chem. Soc.* **2025**, *147* (46), 42701−42710.

(33) Lin, D.; Liu, Y.; Li, Y.; Li, Y.; Pei, A.; Xie, J.; Huang, W.; Cui, Y. Fast Galvanic Lithium Corrosion Involving a Kirkendall-Type Mechanism. *Nat. Chem.* **2019**, *11* (4), 382−389.

https://doi.org/10.1021/acsenergylett.5c03496
ACS Energy Lett. 2026, 11, 1835−1840